

Gravitational quasi-normal modes of charged spherically symmetric black holes surrounded by quintessence fluid in Rastall gravity

Tongzheng Wang(王同征), Yuhao Cui(崔宇昊), and Kai Lin(林恺)

Citation: Chin. Phys. B, 2025, 34 (**3**): 030401. DOI: 10.1088/1674-1056/ada42c
Journal homepage: http://cpb.iphy.ac.cn; http://iopscience.iop.org/cpb

What follows is a list of articles you may be interested in

Triple points and phase transitions of *D*-dimensional dyonic AdS black holes with quasitopological electromagnetism in Einstein-Gauss-Bonnet gravity

Ping-Hui Mou(牟平辉), Qing-Quan Jiang(蒋青权), Ke-Jian He(何柯腱), and Guo-Ping Li(李国平)
Chin. Phys. B, 2024, 33 (**6**): 060401. DOI: 10.1088/1674-1056/ad3342

View of thermodynamic phase transition of the charged Gauss—Bonnet AdS black hole via the shadow

Ke-Jian He(何柯腱), Sen Guo(郭森), Zhi Luo(罗智), and Guo-Ping Li(李国平)
Chin. Phys. B, 2024, 33 (**4**): 040403. DOI: 10.1088/1674-1056/ad225d

The shadow and observation appearance of black hole surrounded by the dust field in Rastall theory

Xuan-Ran Zhu(朱轩然), Yun-Xian Chen(陈芸仙), Ping-Hui Mou(牟平辉), and Ke-Jian He(何柯腱)
Chin. Phys. B, 2023, 32 (**1**): 010401. DOI: 10.1088/1674-1056/ac6ee0

Thermodynamics and weak cosmic censorship conjecture of charged AdS black hole in the Rastall gravity with pressure

Xin-Yun Hu(胡馨匀), Ke-Jian He(何柯健), Zhong-Hua Li(李中华), Guo-Ping Li(李国平)
Chin. Phys. B, 2020, 29 (**5**): 050401. DOI: 10.1088/1674-1056/ab7daa

Gravitational quasi-normal modes of static R^2 Anti-de Sitter black holes

Hong Ma(马洪), Jin Li(李瑾)
Chin. Phys. B, 2017, 26 (**6**): 060401. DOI: 10.1088/1674-1056/26/6/060401

Gravitational quasi-normal modes of charged spherically symmetric black holes surrounded by quintessence fluid in Rastall gravity

Tongzheng Wang(王同征), Yuhao Cui(崔宇昊), and Kai Lin(林恺)†

School of Geophysics and Geomatics, China University of Geosciences, Wuhan 430074, *China*

(Received 9 September 2024; revised manuscript received 17 December 2024; accepted manuscript online 31 December 2024)

We apply the WKB approximation method, matrix method, and finite difference method to study the gravitational quasi-normal modes of charged spherically symmetric black holes surrounded by quintessence fluid in Rastall gravity. By comparing the spherically symmetric spacetime metric of charged black holes surrounded by quintessence fluid in Rastall gravity with that of general relativity, we can find that the modifications to general relativity in this modified gravity theory can be described by parameters such as λ, Q, and $C_{\rm a}$, etc. In four-dimensional spacetime, we investigate the impact of charge Q and parameter $C_{\rm a}$ on the gravitational quasi-normal modes of charged black holes surrounded by quintessence field in Rastall gravity. The aim is to search for observational evidence of such black holes in astrophysical observations and, consequently, test the validity of Rastall theory. In five-dimensional (5D) spacetime, we study the impact of the parameter $C_{\rm a}$ on the gravitational quasi-normal modes of Rastall black holes surrounded by quintessence field and summarize the corresponding variation patterns.

Keywords: quasi-normal modes, Rastall gravity, higher-dimensional

PACS: 04.50.Kd, 04.25.Nx, 04.80.Cc, 04.20.Ha

DOI: 10.1088/1674-1056/ada42c **CSTR:** 32038.14.CPB.ada42c

1. Introduction

Experimental detection of gravitational waves originated in 1960 when Joseph Weber designed and built the first gravitational wave detector.[1] After decades of effort by scientists, in September 2015, humanity achieved its first direct detection of gravitational waves using the Laser Interferometer Gravitational-Wave Observatory (LIGO).[2] This marked the beginning of the era of gravitational wave astronomy. The event not only directly confirmed the existence of gravitational waves but also demonstrated the presence of black holes in the universe. The direct observation of gravitational waves has advanced the development of gravitational wave theories[3–5] and detection technologies.[6–8] The gravitational wave signal was generated during the merger of two massive black holes. Gravitational waves can arise not only from binary compact star mergers but also during the inspiral and ring-down phases of binary compact stars. The ring-down signal holds valuable information about the properties of compact stars and gravitational theories, making it an area of significant research interest. In this article, we investigate the ring-down gravitational waves of charged spherically symmetric black holes surrounded by quintessence fluid in Rastall gravity theory. The ring-down phase of gravitational waves can be studied and computed using quasi-normal modes (QNMs) theory.

General relativity successfully explained the perihelion precession of Mercury[9] and made correct predictions, such as black holes[10] and gravitational waves,[2] etc. However, recent research has revealed that general relativity cannot account for dark matter and dark energy observed through observations.[11–15] Additionally, it is non-renormalizable, making it challenging to quantize using traditional quantum physics methods. One solution to these issues is to introduce modified gravity theories. Some notable modified gravity theories include: Rastall gravity,[16,17] $f(R)$ gravity,[18,19] Gauss–Bonnet gravity,[20–24] $f(T)$ gravity,[25,26] Einstein–Aether gravity,[27] Horava–Lifshitz gravity,[28–30] Kaluza–Klein gravity,[31,32] brane world gravity,[33,34] and scalar-tensor gravity.[35,36] These theories explore different avenues to address the challenges posed by dark matter, dark energy, and the limitations of general relativity.

In 1972, Peter Rastall proposed a modified theory of gravity based on Einstein's gravitational theory. According to Rastall's theory, in curved spacetime, the divergence of the energy–momentum tensor is proportional to the gradient of the Ricci scalar.[16] This theory is known as Rastall gravity. In recent years, Rastall gravity has been extensively studied and applied to various astrophysical contexts. It has been used in neutron star research,[37] wormhole studies,[38] and black hole investigations.[39–41] Additionally, Rastall gravity performs well in stellar model theories.[42,43] Researchers have explored its thermodynamics,[44] shadow and observation appearance,[45] quintessence anisotropic stellar models,[46] spherically symmetric gravitational col-

†Corresponding author. E-mail: lk314159@hotmail.com

© 2025 Chinese Physical Society and IOP Publishing Ltd. All rights, including for text and data mining, AI training, and similar technologies, are reserved.

lapse of a homogeneous perfect fluid,[47] and even its Lagrangian formulation.[48,49] Furthermore, Rastall gravity allows for accelerated cosmic expansion and supports cosmic inflation.[50–55]

The ring-down process can be described by the quasi-normal oscillations of black holes. During this phase, the behavior is solely determined by the black hole's intrinsic properties. The waveform exhibits a distinct feature: spacetime oscillations can be characterized by a fixed complex frequency. The real part of this complex frequency corresponds to the oscillation frequency, while the imaginary part is typically negative, indicating the rate of amplitude decay. These oscillations are known as QNMs in the narrow sense. In 1970, Vishveshwara conducted pioneering research on QNMs of Schwarzschild black holes.[56] The initial perturbation of a black hole becomes a decaying oscillation dominated by a certain frequency after a period of time. The frequency and decaying of oscillation depend only on some parameters of the black hole, such as mass, charge, and angular momentum, etc., and are independent of the initial perturbation that excited this oscillation. Common methods for studying QNMs include finite difference methods,[57] continued fraction methods,[58] WKB approximation methods,[59–63] and matrix methods.[64–66] Among the methods used for studying gravitational waves during the ring-down phase, the WKB approximation methods is computationally efficient and relatively good accuracy. Finite difference methods allow visualization of amplitude changes throughout the entire perturbation process, applicable not only to static black holes but also to dynamic ones. Additionally, matrix methods offer a versatile approach for computing QNMs in various spacetime scenarios and are highly effective for studying gravitational waves associated with ring-down phases.

Studying gravitational waves during the ring-down phase provides valuable insights into the structure and properties of compact stars. Gravitational waves exist not only in four-dimensional (4D) spacetime but theoretically also in higher-dimensional spacetime. High-dimensional theories have been extensively explored within string theory.[67–69] In experimental contexts, researchers have focused on detecting extra dimensions using high-energy experiments, with indications that high-dimensional black holes could be produced in colliders.[70] Observing gravitational waves offers a new avenue for detecting extra dimensions. Studying the gravitational QNMs of black holes in higher-dimensional spacetimes can help us understand the properties of higher-dimensional black holes.

In the second section, we review the solutions of higher-dimensional charged black holes surrounded by quintessence fluid in Rastall gravity and the master equations for gravitational perturbations of spherically symmetric black hole in higher dimensions. In the third section, we study the gravitational QNMs of charged Rastall black holes surrounded by quintessence fluid in 4D spacetime using the WKB approximation methods, matrix methods, and finite difference methods. In the fourth section, we investigate the gravitational QNMs of Rastall black holes surrounded by quintessence fluid in 5D spacetime, in the fifth section, we summarize the article.

2. Charged black hole solutions in Rastall gravity and gravitational perturbation in higher dimensions

In 1972, Perer Rastall proposed that in curved spacetime, the conservation of the energy–momentum tensor does not necessarily manifest as a vanishing covariant derivative. In fact, existing experiments only support the conclusion of a zero ordinary derivative in flat spacetime. The conservation in curved spacetime could take on more complex forms; for instance, one possible scenario is that the divergence of the energy–momentum tensor is proportional to the gradient of the Ricci scalar,[16]

$$T^{\nu}_{\mu;\nu} = \lambda R_{;\mu}, \tag{1}$$

where R is the Ricci scalar and λ is the Rastall parameter. Under this assumption, we can rewrite the Einstein equations with a cosmological constant as follows:

$$R_{\mu\nu} - \frac{1}{2} g_{\mu\nu} R + g_{\mu\nu}\Lambda = \kappa(T_{\mu\nu} - \lambda g_{\mu\nu} R), \tag{2}$$

where Λ represents the cosmological constant, κ is a constant, and $T_{\mu\nu}$ takes the form

$$T_{\mu\nu} = E_{\mu\nu} + T^{*}_{\mu\nu}. \tag{3}$$

The $E_{\mu\nu}$ is the energy–momentum tensor of the electromagnetic field, which can be expressed as

$$E^{\nu}_{\mu} = -(-\xi)^{s}(\mathcal{F})^{s-1}\left(2sF_{\eta\mu}F^{\eta\nu} - \frac{1}{2}\delta^{\nu}_{\mu}\mathcal{F}\right). \tag{4}$$

From an electrodynamic perspective, the self-energy of a point-like charge diverges at the origin. To address this singularity, Born and Infeld introduced a novel form of nonlinear electrodynamics in 1934.[71] In 1935, Hoffmann coupled nonlinear electrodynamics with gravity.[72] Power Maxwell field is a type model of nonlinear electrodynamics. An appealing aspect of the power Maxwell theory is its ability to maintain conformal invariance when the exponent of the Maxwell invariant equals one-fourth of the spacetime dimensions.[73] The action for the electromagnetic field can be described by a nonlinear form[74]

$$\mathcal{L}_{\mathrm{F}} = -(-\xi\mathcal{F})^{s}, \tag{5}$$

where $\mathcal{F}=F_{\mu\nu}F^{\mu\nu}$, $F_{\mu\nu}=A_{\mu;\nu}-A_{\nu;\mu}$ is the Faraday tensor, A_μ is the vector potential, and ξ and s are constants. In this article, we only consider the case of $s=1$.

To address the problem of dark energy, the simplest model is to describe dark energy using the cosmological constant, known as the ΛCDM model (including vacuum energy and cold dark matter), with the corresponding equation of state being $w=p/\rho=-1$.[75] In addition to introducing the cosmological constant, dark energy can be described using a slowly evolving scalar field, such as quintessence,[76] k-essence,[77] tachyon,[78] phantom,[79] or quintom.[80] Besides the ΛCDM cosmological model, another option is the QCDM model, which incorporates quintessence and cold dark matter. From Ref. [81], the components of the quintessence fluid $T^*_{\mu\nu}$ can be expressed as

$$T^{*t}_{t}=T^{*r}_{r}=-\rho(r), \tag{6}$$

$$T^{*\theta_1}_{\theta_1}=T^{*\theta_2}_{\theta_2}=\frac{1}{D-2}\rho(r)\left[(D-1)w_{\rm q}+1\right], \tag{7}$$

where D represents the dimension of spacetime, ρ is the density of the quintessence fluid, and the relationship between the pressure p and the density ρ is given by $p=w_{\rm q}\rho$, where $w_{\rm q}$ is the state parameter of quintessence, with a range of $-1<w_{\rm q}<0$.

In 2019, the black hole solutions in higher-dimensional spacetimes with the presence of the power-Maxwell field, surrounded by quintessence, are investigated in Rastall gravity.[17] The solution takes the following form:

$$\begin{aligned}f(r)=1&-\frac{8\Gamma(\frac{D-1}{2})M_{\rm a}}{\pi^{\frac{D-3}{2}}(D-2)r^{D-3}}+\frac{2\Lambda r^2}{(D-1)\left[2\kappa\lambda D-D+2\right]}+\frac{4Q^2\Gamma(\frac{D-1}{2})(2s-1)^{\frac{D-1-2s}{1-2s}}r^{\frac{2(D-4)s+2}{1-2s}}}{\pi^{\frac{D-3}{2}}(D-2)s(D-1-2s)}\\&-\frac{2\kappa C_{\rm a}\left\{(D-1)\left[2\kappa\lambda(w_{\rm q}+1)-1\right]+1\right\}^2}{(D-2)(D-1)\left[2\kappa\lambda D-D+2\right]}\frac{r^{-\frac{(D-2)[(D-1)(w_{\rm q}+1)(2\kappa\lambda-1)+2]}{(D-1)[2\kappa\lambda(w_{\rm q}+1)-1]+1}}}{(D-2)w_{\rm q}-2\kappa\lambda(w_{\rm q}+1)},\end{aligned} \tag{8}$$

$$\rho=C_{\rm a}r^{\frac{(D-1)[2\kappa\lambda(w_{\rm q}+1)-1]+1}{(D-1)(w_{\rm q}+1)[2\kappa\lambda D-D+2]}}-\frac{8\lambda\pi^{\frac{3-D}{2}}Q^2(D-4s)(2s-1)^{\frac{D-1-2s}{1-2s}-2}\Gamma(\frac{D-1}{2})}{\left\{(D-1)\left[(2s-1)w_{\rm q}-1\right]+2s\right\}r^{\frac{2(D-2)s}{2s-1}}}, \tag{9}$$

where $M_{\rm a}$ is related to the mass of the black hole. The presence of $C_{\rm a}$ is associated with the consideration of the quintessence fluid. $C_{\rm a}$ represents the structure parameter of the quintessence fluid.

In 1957, Regge and Wheeler investigated gravitational perturbations in the Schwarzschild spacetime using metric perturbations and analyzed the stability of Schwarzschild black holes.[82] Subsequently, Zerilli and Moncrief contributed to the study of gravitational perturbations.[83,84] Teukolsky further explored gravitational perturbations in the Kerr spacetime.[85] In 2010, in Ref. [86], the authors studied the gravitational field perturbations of higher-dimensional spherically symmetric black holes and obtained the master equations for tensor-type, vector-type, and scalar-type gravitational perturbations. For spherically symmetric black holes, the perturbation equations can be cast into a Schrodinger-like form

$$-\frac{{\rm d}^2\Psi}{{\rm d}r_*^2}+V(r(r_*))\Psi=\omega^2\Psi, \tag{10}$$

where r_* represents the tortoise coordinate defined as $r_*\equiv\int 1/f(r)\,{\rm d}r$.

In the solution of tensor-type gravitational field perturbations, the metric perturbation has the following form:

$$\delta g_{\mu\nu}=\left(\begin{array}{cc|c}0&0&0\\0&0&0\\\hline 0&0&r^2\varphi T_{ij}\end{array}\right), \tag{11}$$

where φ corresponds to the master variable, and T_{ij} is the tensor harmonics. The effective potential for tensor-type gravitational perturbations is given by[86]

$$V_t(r)=\frac{(2\kappa+\gamma_t)f}{(D-4)r}\frac{{\rm d}\ln T'}{{\rm d}r}+\frac{1}{r\sqrt{T'}}f\frac{\rm d}{{\rm d}r}\left(f\frac{\rm d}{{\rm d}r}r\sqrt{T'}\right), \tag{12}$$

where $\gamma_t=L(L+D-3)-2$, $(L=2,3,4,\ldots)$,

$$T(r)=\int r^{D-4}\,{\rm d}r. \tag{13}$$

With the choice of the Regge–Wheeler gauge, the metric perturbation takes the following form:

$$\delta g_{\mu\nu}=\left(\begin{array}{cc|c}0&0&v_i\\0&0&w_i\\\hline v_i&w_i&\mathbf{0}\end{array}\right). \tag{14}$$

In this expression, v_i and w_i satisfy the condition: $\nabla^i v_i=\nabla^i w_i=0$. For vector-type perturbations, the effective potential is[86]

$$V_{\rm v}(r)=r\sqrt{T'}f\partial_r\left(f\partial_r\frac{1}{r\sqrt{T'}}\right)+\left(\frac{\gamma_v}{D-3}-\kappa\right)\frac{fT'}{rT}, \tag{15}$$

where $\gamma_v=L(L+D-3)-1$, $(L=2,3,4,\ldots)$.

After choosing the Zerilli gauge, the metric perturbation has the following form:

$$\delta g_{\mu\nu}=\left(\begin{array}{cc|c}f\overline{H}&H_1&0\\H_1&H/f&0\\\hline 0&0&r^2K\overline{\gamma}_{ij}\end{array}\right), \tag{16}$$

all perturbation variables $\overline{H}$, H_1, H, and K are related to the master function ϕ. For scalar-type perturbations, the effective potential is[86]

$$V_{\rm s}(r) = 2\gamma_{\rm s} f\frac{(rNT)'}{(D-2)NTr^2} - \frac{f}{N}\partial_r(f\partial_r N) + 2f^2\frac{N'^2}{N^2} - \frac{f}{T}\partial_r(f\partial_r T) + 2f^2\frac{T'^2}{T^2} + 2f^2\frac{N'T'}{NT}, \tag{17}$$

where $\gamma_{\rm s} = L(L+D-3)$, $(L=2,3,4,\ldots)$,

$$N = \frac{A}{r\sqrt{T'}}, \quad A(r) = -2(D-2)f + 2\gamma_{\rm s} + (D-2)rf'. \tag{18}$$

Next, we will investigate the gravitational QNMs of Rastall black holes surrounded by quintessence fluid in 4D and 5D spacetimes.

3. Numerical results in 4D spacetime

Using the WKB approximation method, matrix method, and finite difference method, we first investigate the impact of charge Q on the gravitational QNMs of the charged black hole surrounded by quintessence fluid in Rastall gravity. In 4D spacetime, $D=4$, we take $\Lambda=0$, $\kappa=1$, $C_{\rm a}=1$, $s=1$, $w_{\rm q}=-2/3$, $\lambda=4$. The metric simplifies to

$$f(r) = 1 - \frac{2M_{\rm a}}{r} + \frac{Q^2}{r^2} + \frac{1}{10r^3}. \tag{19}$$

When the metric takes the form of Eq. (19), we find that there are two positive real roots and one negative root in the solutions of $f(r)=0$. The metric $f(r)$ has the following form:

$$f(r) = \left(1-\frac{r_{\rm p}}{r}\right)\left(1-\frac{C_{\rm ri}r_{\rm p}}{r}\right)\left(1+\frac{\mathscr{A}}{r}\right), \tag{20}$$

where $\mathscr{A}$ and $C_{\rm ri}$ are respectively

$$\mathscr{A} = \frac{-1-10Q^2r_{\rm p}+\sqrt{40r_{\rm p}^3+(1+10Q^2r_{\rm p})^2}}{20r_{\rm p}^2}, \quad C_{\rm ri} = \frac{1+10Q^2r_{\rm p}+\sqrt{40r_{\rm p}^3+(1+10Q^2r_{\rm p})^2}}{20r_{\rm p}^3}, \tag{21}$$

$r_{\rm p}$ is the event horizon, $r_{\rm i} \equiv C_{\rm ri}r_{\rm p}$ is the inner horizon. The condition $0 < C_{\rm ri} < 1$ restricts the range of charge Q to

$$-\frac{\sqrt{-1+5r_{\rm p}^3}}{\sqrt{5r_{\rm p}}} < Q < \frac{\sqrt{-1+5r_{\rm p}^3}}{\sqrt{5r_{\rm p}}}.$$

The WKB approximation methods is a semi-analytical method. According to this method, the eigenvalue of the complex frequencies are given by

$$\frac{{\rm i}(\omega^2-V)}{\sqrt{-2V''}}\Big|_{r=x_0} = n + \frac{1}{2} + \sum_{j=2}\Lambda_j, \tag{22}$$

x_0 corresponds to the coordinate where the potential V reaches its maximum, and Λ_j is the correction term of the WKB approximation methods.

To ensure the accuracy of the calculations, we also utilize matrix methods to compute QNMs frequencies. With matrix methods, we can assume that the function $\Psi(r)$ in Eq. (10) has the following form:

$$\Psi(r) = (r-r_{\rm p})^{-{\rm i}\omega r_{\rm p}}\,{\rm e}^{{\rm i}\omega(r-r_{\rm p})}r^{2{\rm i}\omega r_{\rm p}}\Phi(r). \tag{23}$$

As a result, $\Phi(r)$ is regular both at the event horizon and at infinity. Next, we introduce the transformation: $x = 1 - r_{\rm p}/r$. Thus, at the event horizon, $x=0$, and at infinity, $x=1$. Then, by selecting N points in the interval $x\in[0,1]$ and utilizing high-precision difference methods, we can express the field equation as a matrix equation

$$\mathcal{G}(\omega)\mathcal{F} = 0, \tag{24}$$

where $\mathcal{G}(\omega)$ is an $N\times N$ matrix, and $\mathcal{F}$ is an $N\times 1$ column matrix representing the values of $\Phi(x_i)$ at N selected points $x_{\rm i}$. Finally, by calculating the determinant

$$\det\left(\mathcal{G}(\omega)\right) = 0. \tag{25}$$

The eigenvalues ω can be determined by computing the determinant. Clearly, to improve accuracy, one simply needs to increase the number of sample points N within the interval $x\in[0,1]$.

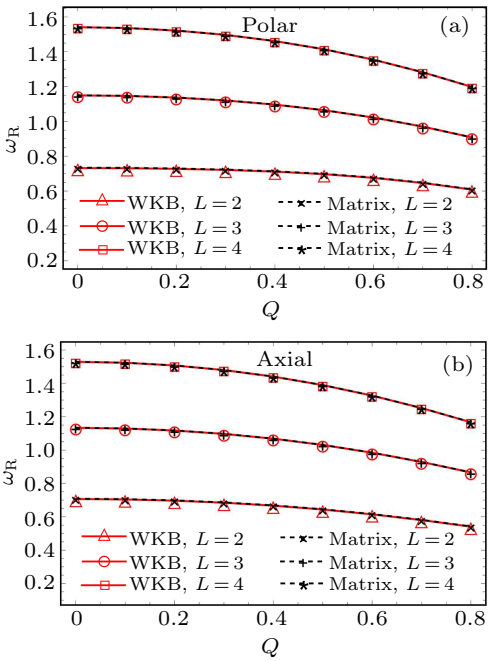


Fig. 1. The real part of the polar (a) and axial (b) gravitational QNMs as functions of parameter Q with $r_{\rm p}=1$ and $n=0$.

We used the third-order WKB approximation methods and the matrix method for the case of $N=22$ to calculate the polar and axial gravitational QNMs of charged black holes surrounded by quintessence fluid in Rastall gravity when the

metric takes the form of Eq. (19) (where scalar-type perturbations in higher-dimensional spacetime correspond to polar gravitational perturbations in 4D spacetime, and vector-type perturbations in higher-dimensional spacetime correspond to axial gravitational perturbations in 4D spacetime). The results are shown in Figs. 1 and 2, where figure 1 shows the real part of the QNMs as a function of the charge Q, and figure 2 shows the absolute value of the imaginary part of the QNMs as a function of the charge Q. From these results, we can see that as the charge Q increases, both the real part and the absolute value of the imaginary part of the QNMs decrease. This means that when the metric takes the form of Eq. (19), as the charge Q of the black hole increases, the oscillation frequency decreases, and the amplitudes decay more slowly. Additionally, as the angular quantum number L increases, both the real part and the absolute value of the imaginary part of the QNMs frequency increase.

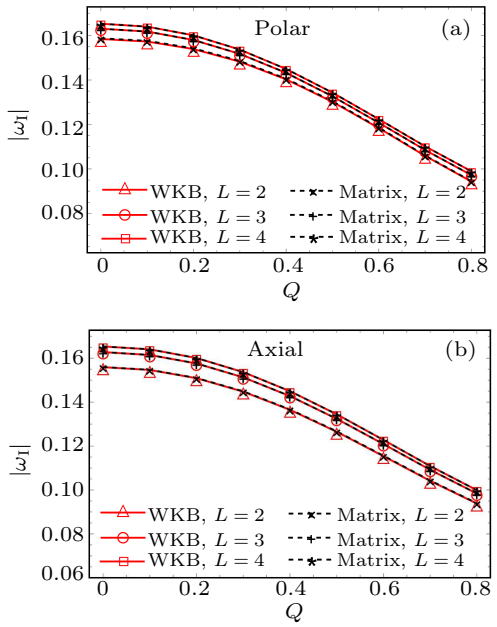


Fig. 2. The absolute value of the imaginary part of the polar (a) and axial (b) gravitational QNMs as functions of parameter Q with $r_{\rm p}=1$ and $n=0$.

Next, we used finite-difference methods to compute the gravitational QNMs of Rastall black holes surrounded by quintessence fluid. By introducing coordinate transformations $u=t-r_*, v=t+r_*$. The main equation becomes

$$4\frac{\partial^2\Psi}{\partial u\partial v}+V(r)\Psi=0, \tag{26}$$

which we discretize from a differential equation into a difference equation. The above equation is reduced to

$$\Psi_N\approx\Psi_E+\Psi_W-\Psi_S-\Delta u\Delta v\frac{\Psi_E+\Psi_W}{8}V(r), \tag{27}$$

where Ψ represents the value at the discretized point (a,b), and we can denote the Ψ on this point as $\Psi_{a,b}$. Then the above equation

$$\begin{aligned}&\Psi_N=\Psi_{a+1,b+1}, \quad \Psi_S=\Psi_{a-1,b-1},\\ &\Psi_E=\Psi_{a+1,b-1}, \quad \Psi_W=\Psi_{a-1,b+1},\end{aligned} \tag{28}$$

$$\begin{aligned}&\Delta u\approx u_N-u_E=u_W-u_S,\\ &\Delta v\approx v_N-v_E=v_W-v_S.\end{aligned} \tag{29}$$

If we know the values of Ψ at points E, W, and S, we can compute the value of Ψ at point N by solving the difference equation. The initial conditions and boundary conditions are given by

$$\begin{aligned}&\Psi(u=u_0,v)=\exp\left[-\frac{(v-v_{\rm c})^2}{2\sigma^2}\right],\\ &\Psi(u,v=v_0)=0,\end{aligned} \tag{30}$$

where u_0, v_0, σ, and $v_{\rm c}$ correspond to specific forms of the initial Gaussian waveform and the boundary. In this article, all the finite difference method images are plotted based on the Ψ values along the r_*-t diagonal.

The results of the finite difference method are shown in Fig. 3. We can see that as the charge Q increases, the oscillation frequency decreases, and the amplitude decays more slowly. This is consistent with the results calculated using the WKB approximation method and the matrix method.

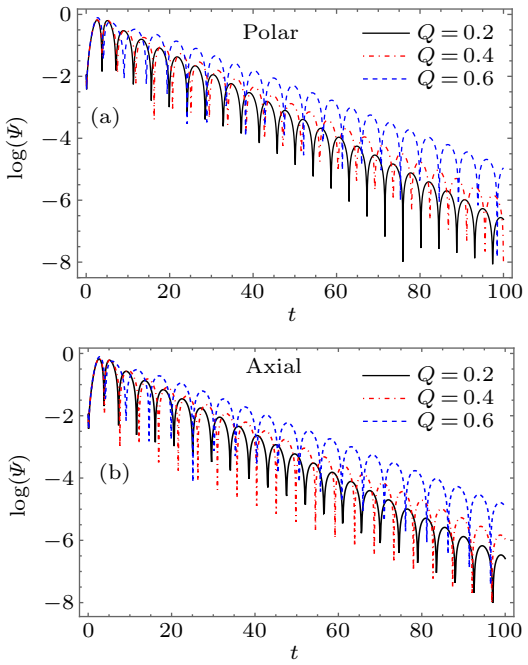


Fig. 3. Wave function images for the polar (a) and axial (b) gravitational perturbation with $r_{\rm p}=1$ and $L=2$.

Subsequently, we studied the effect of the parameter $C_{\rm a}$ on the QNMs. In 4D spacetime, $D=4$, we take $\Lambda=0$, $\kappa=1$, $w_{\rm q}=-2/3$, $\lambda=2$, $Q=0$. The metric simplifies to

$$f(r)=1-\frac{2M_{\rm a}}{r}+\frac{C_{\rm a}}{28r^5}. \tag{31}$$

We divide the solutions into two different cases based on the properties of the horizons which are governed by $f(r)=0$.

Case 1 The solution of $f(r)=0$ has only one positive real root as the event horizon $r_{\rm p}$, and $f(r)$ has the following form:

$$f(r)=(1-\frac{r_{\rm p}}{r})\left(1+\frac{\mathscr{B}}{r}+\frac{\mathscr{C}}{r^2}+\frac{\mathscr{D}}{r^3}+\frac{\mathscr{E}}{r^4}\right), \tag{32}$$

where $\mathscr{B}$, $\mathscr{C}$, $\mathscr{D}$, and $\mathscr{E}$ are parameters, given by

$$\begin{aligned}&\mathscr{B}=-\frac{C_{\rm a}}{28r_{\rm p}^4},\quad \mathscr{C}=-\frac{C_{\rm a}}{28r_{\rm p}^3},\quad \mathscr{D}=-\frac{C_{\rm a}}{28r_{\rm p}^2},\\ &\mathscr{E}=-\frac{C_{\rm a}}{28r_{\rm p}},\quad M_{\rm a}=\frac{C_{\rm a}+28r_{\rm p}^5}{56r_{\rm p}^4}.\end{aligned} \tag{33}$$

To ensure that

$$1+\frac{\mathscr{B}}{r}+\frac{\mathscr{C}}{r^2}+\frac{\mathscr{D}}{r^3}+\frac{\mathscr{E}}{r^4}=0$$

has only negative and complex roots, we need the condition $C_{\rm a}<0$.

Case 2 The solution of $f(r)=0$ has two positive real roots: one at the event horizon $r_{\rm p}$ and the other at the inner horizon $r_{\rm i}\equiv C_{\rm ri}r_{\rm p}$. In this case, $f(r)$ has the following form:

$$f(r)=\left(1-\frac{r_{\rm p}}{r}\right)\left(1-\frac{C_{\rm ri}r_{\rm p}}{r}\right)\left(1+\frac{\mathscr{F}}{r}+\frac{\mathscr{G}}{r^2}+\frac{\mathscr{H}}{r^3}\right), \tag{34}$$

where $\mathscr{F}$, $\mathscr{G}$, and $\mathscr{H}$ are parameters, given by

$$\begin{aligned}&\mathscr{F}=\frac{C_{\rm ri}(1+C_{\rm ri}+C_{\rm ri}^2)r_{\rm p}}{1+C_{\rm ri}+C_{\rm ri}^2+C_{\rm ri}^3},\quad \mathscr{G}=\frac{C_{\rm ri}^2r_{\rm p}^2}{1+C_{\rm ri}^2},\\ &\mathscr{H}=\frac{C_{\rm ri}^3r_{\rm p}^3}{1+C_{\rm ri}+C_{\rm ri}^2+C_{\rm ri}^3},\\ &C_{\rm a}=\frac{28C_{\rm ri}^4r_{\rm p}^5}{1+C_{\rm ri}+C_{\rm ri}^2+C_{\rm ri}^3},\\ &M_{\rm a}=\frac{r_{\rm p}+C_{\rm ri}r_{\rm p}+C_{\rm ri}^2r_{\rm p}+C_{\rm ri}^3r_{\rm p}+C_{\rm ri}^4r_{\rm p}}{2(1+C_{\rm ri}+C_{\rm ri}^2+C_{\rm ri}^3)},\end{aligned} \tag{35}$$

where $0<C_{\rm ri}<1$. When $C_{\rm ri}=1$, the black hole becomes an extreme black hole. In this case, from Eq. (35) we can obtain $C_{\rm a}>0$. We found that scenarios with three or more horizons do not exist for this black hole.

We performed calculations using third-order WKB approximation methods and the matrix method for the case of $N=22$. Specifically, for Case 1 with L values of 2, 3, and 4, we investigated the polar and axial gravitational QNMs of Rastall black holes surrounded by quintessence fluid. The results are shown in Figs. 4 and 5. Figure 4 displays the real part of the QNMs as a function of the parameter $C_{\rm a}$, while figure 5 shows the absolute value of the imaginary part of the QNMs as a function of the parameter $C_{\rm a}$. From these results, we can observe that as the parameter $C_{\rm a}$ increases (the absolute value of $C_{\rm a}$ decreases), both the real part and the absolute value of the imaginary part of the QNMs frequencies decrease.

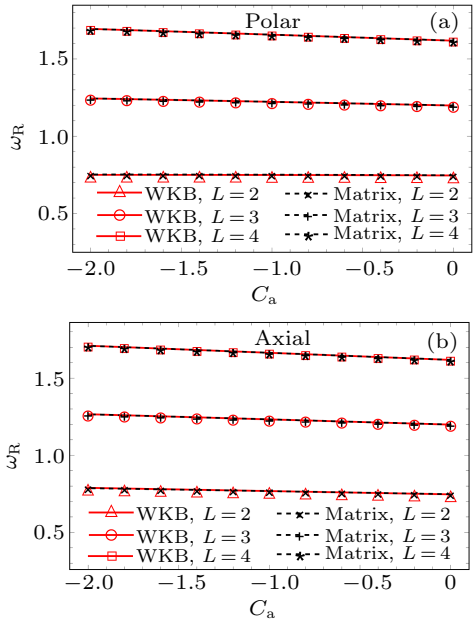


Fig. 4. The real part of the polar (a) and axial (b) gravitational QNMs as functions of parameter $C_{\rm a}$ for Case 1 with $r_{\rm p}=1$ and $n=0$.

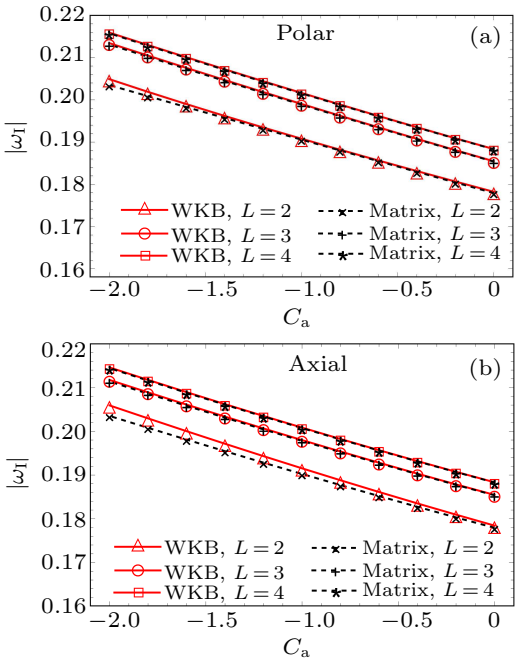


Fig. 5. The absolute value of the imaginary part of the polar (a) and axial (b) gravitational QNMs as functions of parameter $C_{\rm a}$ for Case 1 with $r_{\rm p}=1$ and $n=0$.

Additionally, the real part and the absolute value of the imaginary part of the gravitational QNMs for the black hole in this modified gravity theory are larger than those of Schwarzschild case. This indicates that black holes in this modified gravity theory exhibit higher oscillation frequencies and faster amplitude decay compared to the Schwarzschild black holes. Furthermore, as the angular quantum number L increases, the real part and the absolute values of imaginary part of the QNMs frequencies increase.

The finite difference results are shown in Fig. 6. We can observe that as the parameter $C_{\rm a}$ increases, the oscillation fre-

quency decreases, and the amplitudes decay more slowly. This behavior is consistent with the results obtained using the WKB approximation method and the matrix method. And it can be observed that in this modified gravity, the late-time tail occurs earlier compared to the Schwarzschild case. Furthermore, as the absolute value of the parameter $C_{\rm a}$ increases, the tail appears even earlier.

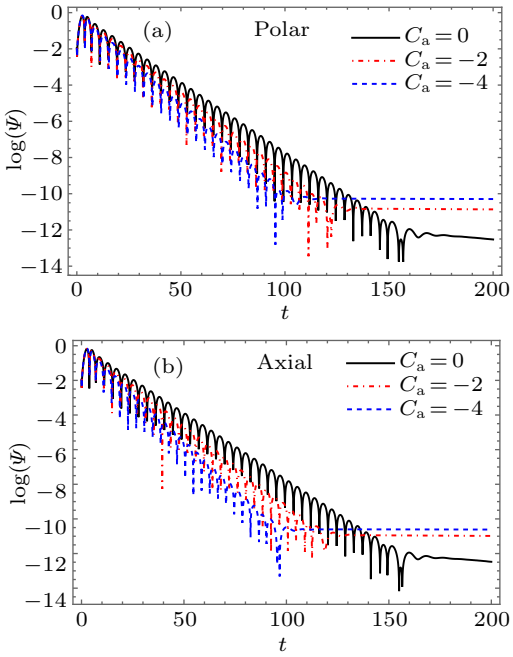


Fig. 6. Wave function images for the polar (a) and axial (b) gravitational perturbation for Case 1 with $r_{\rm p}=1$ and $L=2$.

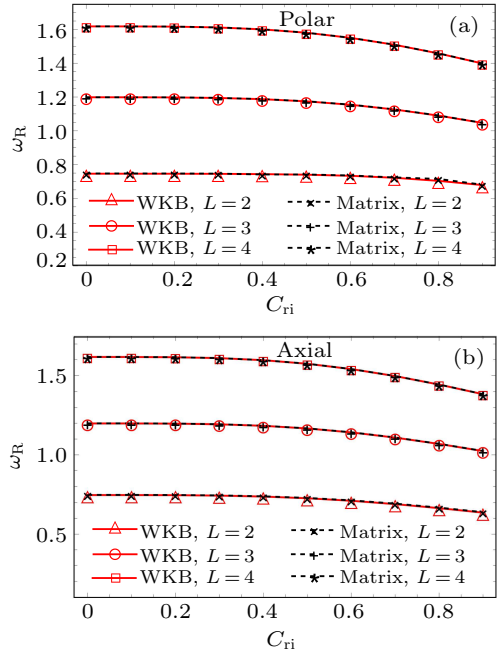


Fig. 7. The real part of the polar (a) and axial (b) gravitational QNMs varies with the parameter $C_{\rm ri}$ for Case 2 with $r_{\rm p}=1$ and $n=0$.

In Case 2, we discuss the impact of changes in the black hole's inner horizon on the QNMs. The QNMs calculations for polar and axial gravitational perturbations are shown in Figs. 7 and 8, respectively. Figure 7 displays the real part of the QNMs as the black hole's inner horizon varies, while figure 8 shows the absolute value of the imaginary part of the QNMs as the black hole's inner horizon varies.

From Fig. 7, we observe that the oscillation frequency decreases as the inner horizon of the black hole increases. Figure 8 reveals that the amplitudes decay more slowly as the inner horizon increases. Additionally, as the angular quantum number L increases, both the real and the absolute value of the imaginary part of the QNMs frequency increase.

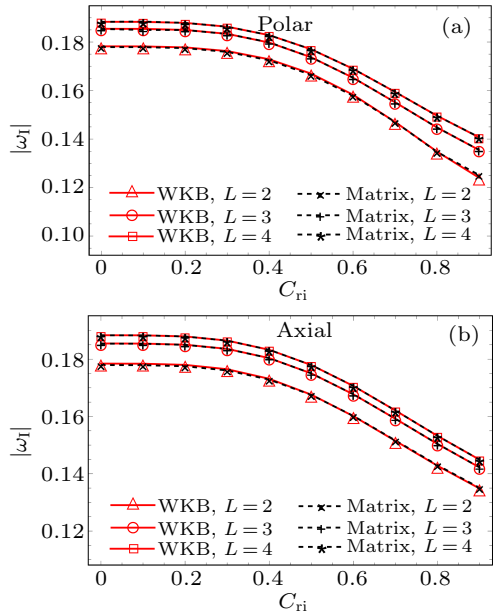


Fig. 8. The absolute value of the imaginary part of the polar (a) and axial (b) gravitational QNMs varies with the parameter $C_{\rm ri}$ for Case 2 with $r_{\rm p}=1$ and $n=0$.

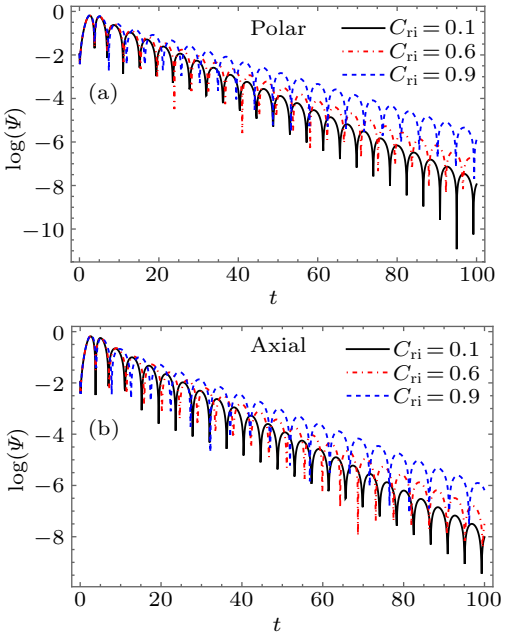


Fig. 9. Wave function images for the polar (a) and axial (b) gravitational perturbation for Case 2 with $r_{\rm p}=1$ and $L=2$.

Table 1. The polar gravitational QNMs obtained by WKB approximation methods and matrix method for extreme black holes of Case 2 with $r_{\rm p}=1$.

L	n	ω (third-order WKB)	ω (sixth-order WKB)	ω (matrix method)
2	0	0.648358 – 0.116561i	0.634191 – 0.127887i	0.651180 – 0.117843i
	1	0.597538 – 0.354919i		0.612024 – 0.359254i
3	0	0.998516 – 0.128158i	0.999259 – 0.128049i	0.999140 – 0.128155i
	1	0.969468 – 0.388532i	0.972186 – 0.386637i	0.971364 – 0.387808i
	2	0.916278 – 0.658826i	0.91884 – 0.651902i	0.931725 – 0.638131i
4	0	1.33385 – 0.133313i	1.33417 – 0.133333i	1.334180 – 0.133339i
	1	1.31082 – 0.402191i	1.31199 – 0.402028i	1.311712 – 0.401241i
	2	1.26695 – 0.677064i	1.26794 – 0.67698i	1.168848 – 0.687223i
5	0	1.66163 – 0.135952i	1.66181 – 0.135959i	1.661829 – 0.135917i
	1	1.64284 – 0.409327i	1.64348 – 0.409255i	1.641696 – 0.412062i
	2	1.60647 – 0.686775i	1.60704 – 0.686761i	1.627788 – 0.618024i

Table 2. The axial gravitational QNMs obtained by WKB approximation methods and matrix method for extreme black holes of Case 2 with $r_{\rm p}=1$.

L	n	ω (third-order WKB)	ω (sixth-order WKB)	ω (matrix method)
2	0	0.605292 – 0.127964i	0.610867 – 0.126464i	0.608348 – 0.128210i
	1	0.548157 – 0.395547i	0.571645 – 0.376145i	0.560691 – 0.391766i
3	0	0.97593 – 0.134973i	0.976711 – 0.134973i	0.976684 – 0.134996i
	1	0.942941 – 0.409435i	0.945744 – 0.408719i	0.946225 – 0.409118i
	2	0.882478 – 0.694771i	0.884941 – 0.694425i	0.868508 – 0.660779i
4	0	1.31835 – 0.137548i	1.31867 – 0.137547i	1.318687 – 0.137560i
	1	1.2941 – 0.415126i	1.29525 – 0.414886i	1.293751 – 0.413852i
	2	1.24809 – 0.69923i	1.2489 – 0.69915i	1.074494 – 0.708515i
5	0	1.64964 – 0.138775i	1.64981 – 0.138775i	1.649814 – 0.138706i
	1	1.6303 – 0.417909i	1.6309 – 0.417807i	1.630556 – 0.423072i
	2	1.59296 – 0.701393i	1.59336 – 0.701368i	1.594879 – 0.609336i

We also plot the wave function images for the inner horizon $r_{\rm i}$ at values of $0.1\cdot r_{\rm p}$, $0.6\cdot r_{\rm p}$, and $0.9\cdot r_{\rm p}$, as shown in Fig. 9. From the figure, we observe that as the inner horizon increases, the oscillation frequency decreases, and the amplitudes decay more slowly. This result is consistent with the calculations obtained using the third-order WKB approximation method and the matrix method.

We further calculate the QNMs for extreme black holes using the WKB approximation methods and matrix methods, as summarized in Tables 1 and 2. Table 1 presents the QNMs for polar gravitational perturbations, while Table 2 shows the QNMs for axial gravitational perturbations. We found that the oscillation frequency decreases with increasing overtone n, and the amplitudes decay more rapidly with increasing overtone n.

4. Numerical results in 5D spacetime

In this section, we investigate the gravitational QNMs of 5D Rastall black holes surrounded by quintessence fluid. We employ the WKB approximation methods, matrix methods, and finite difference methods to study the QNMs.

In the five-dimensional spacetime with $D=5$, we take $\Lambda=0$, $\kappa=1$, $w_{\rm q}=-2/3$, $\lambda=51/16$, $Q=0$, which simplifies the metric to

$$f(r)=1-\frac{8M_{\rm a}}{3\pi r^2}+\frac{8C_{\rm a}}{189r^5}. \tag{36}$$

We divide the solutions into two different cases based on the properties of the horizons which are governed by $f(r)=0$.

Case A The solution of $f(r)=0$ has only one positive real root as the event horizon $r_{\rm p}$, and $f(r)$ has the following form:

$$f(r)=\left(1-\frac{r_{\rm p}}{r}\right)\left(1+\frac{\mathscr{I}}{r}+\frac{\mathscr{J}}{r^2}+\frac{\mathscr{K}}{r^3}+\frac{\mathscr{L}}{r^4}\right), \tag{37}$$

where $\mathscr{I}$, $\mathscr{J}$, $\mathscr{K}$, and $\mathscr{L}$ are parameters, given by

$$\mathscr{I}=r_{\rm p},\quad \mathscr{J}=-\frac{8C_{\rm a}}{189r_{\rm p}^3},\quad \mathscr{K}=-\frac{8C_{\rm a}}{189r_{\rm p}^2},$$
$$\mathscr{L}=-\frac{8C_{\rm a}}{189r_{\rm p}},\quad M_{\rm a}=\frac{8\pi C_{\rm a}+189\pi r_{\rm p}^5}{504r_{\rm p}^3}. \tag{38}$$

To ensure that

$$1+\frac{\mathscr{I}}{r}+\frac{\mathscr{J}}{r^2}+\frac{\mathscr{K}}{r^3}+\frac{\mathscr{L}}{r^4}=0$$

has only negative and complex roots, we need the condition $C_{\rm a}<0$.

Case B There are two positive real roots in the solution of $f(r)=0$, one of which is the event horizon $r_{\rm p}$, and the other

is the inner horizon $r_{\rm i} \equiv C_{\rm ri} r_{\rm p}$. In this case, $f(r)$ has the following form:

$$f(r) = \left(1 - \frac{r_{\rm p}}{r}\right)\left(1 - \frac{C_{\rm ri} r_{\rm p}}{r}\right)\left(1 + \frac{\mathscr{M}}{r} + \frac{\mathscr{N}}{r^2} + \frac{\mathscr{O}}{r^3}\right), \quad (39)$$

where $\mathscr{M}$, $\mathscr{N}$, and $\mathscr{O}$ are parameters, given by

$$\begin{aligned} \mathscr{M} &= r_{\rm p} + C_{\rm ri} r_{\rm p}, \quad \mathscr{N} = \frac{C_{\rm ri}(1+C_{\rm ri})^2 r_{\rm p}^2}{1 + C_{\rm ri} + C_{\rm ri}^2}, \\ \mathscr{O} &= \frac{C_{\rm ri}^2 (1+C_{\rm ri}) r_{\rm p}^3}{1 + C_{\rm ri} + C_{\rm ri}^2}, \quad (40) \\ C_{\rm a} &= \frac{189 C_{\rm ri}^3 (1+C_{\rm ri}) r_{\rm p}^5}{8(1 + C_{\rm ri} + C_{\rm ri}^2)}, \end{aligned}$$

$$M_{\rm a} = \frac{3(1 + C_{\rm ri} + C_{\rm ri}^2 + C_{\rm ri}^3 + C_{\rm ri}^4)\pi r_{\rm p}^2}{8(1 + C_{\rm ri} + C_{\rm ri}^2)}, \quad (41)$$

where $0 < C_{\rm ri} < 1$, and when $C_{\rm ri} = 1$, the black hole becomes an extreme black hole. In this case, from Eq. (40) we can obtain $C_{\rm a} > 0$. We found that black holes with three or more horizons do not exist.

Case A We present the results of calculating the gravitational QNMs frequencies of Rastall black holes surrounded by quintessence fluid using both the third-order WKB approximation method and the matrix method for the case of $N = 22$. The results are shown in Figs. 10 and 11, where figure 10 shows the real part of the QNMs as a function of the parameter $C_{\rm a}$, and figure 11 shows the absolute value of the imaginary part of the QNMs as a function of the parameter $C_{\rm a}$. From Fig. 10, we can see that the oscillation frequency decreases with the increase of the parameter $C_{\rm a}$. From Fig. 11, we can see that the amplitude decay of the oscillation slows down with the increase of the parameter $C_{\rm a}$.

Case A The finite difference results are shown in Fig. 12. We observe that as the parameter $C_{\rm a}$ increases, the oscillation frequency decreases, and the amplitudes decay more slowly, which is consistent with the results of the WKB approximation method and the matrix method.

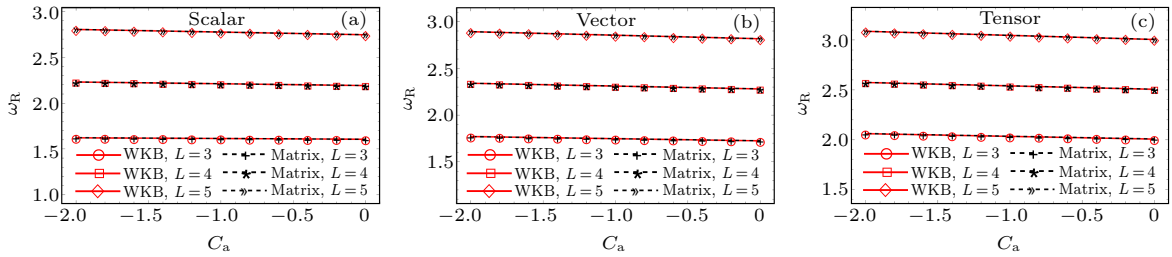


Fig. 10. The real part of the scalar-type (a), vector-type (b), and tensor-type (c) gravitational QNMs as functions of parameter $C_{\rm a}$ for Case A with $r_{\rm p} = 1$ and $n = 0$.

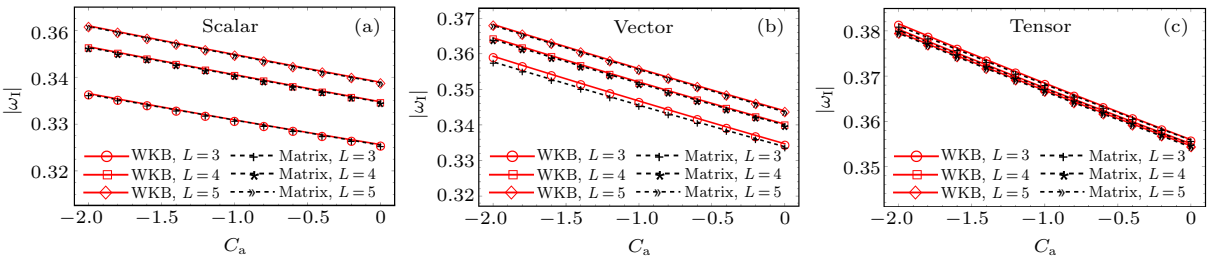


Fig. 11. The absolute value of the imaginary part of the scalar-type (a), vector-type (b), and tensor-type (c) gravitational QNMs as functions of parameter $C_{\rm a}$ for Case A with $r_{\rm p} = 1$ and $n = 0$.

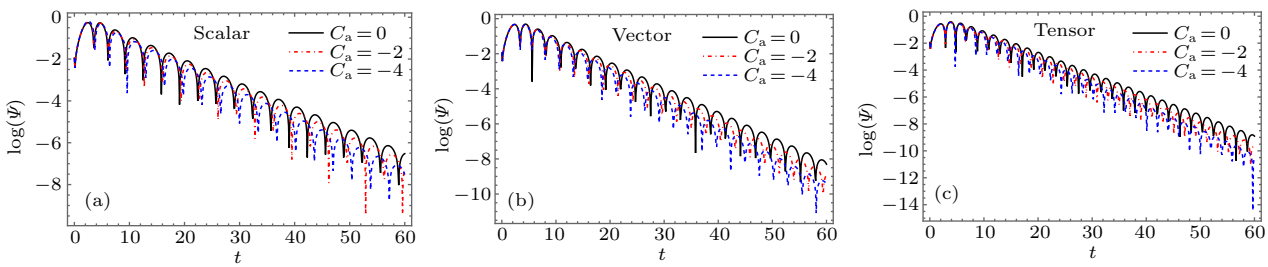


Fig. 12. Wave function images of the scalar-type (a), vector-type (b), and tensor-type (c) gravitational perturbation for Case A with $r_{\rm p} = 1$ and $L = 2$.

Case B We further analyze the behavior of the gravitational QNMs concerning variations in the inner horizon position. We calculate the QNMs using the WKB approximation methods and matrix methods for scalar-type, vector-type, and tensor-type gravitational perturbations. Figure 13 displays the real part of the QNMs as the black hole's inner horizon varies, while figure 14 shows the absolute value of the imaginary part of the QNMs as the black hole's inner hori-

zon varies. From Fig. 13, we observe that the real part of the QNMs decreases as the inner horizon increases. This behavior indicates that the oscillation frequency decreases with an increasing inner horizon. Figure 14 shows that the absolute value of the imaginary part of the QNMs decreases as the inner horizon increases. This indicates that the amplitudes decay more slowly with an increasing inner horizon of the black hole. As the angular quantum number L increases, the real part of the QNMs frequency increases. We find that the absolute value of the imaginary part of the tensor-type gravitational QNMs is not significantly sensitive to changes in L.

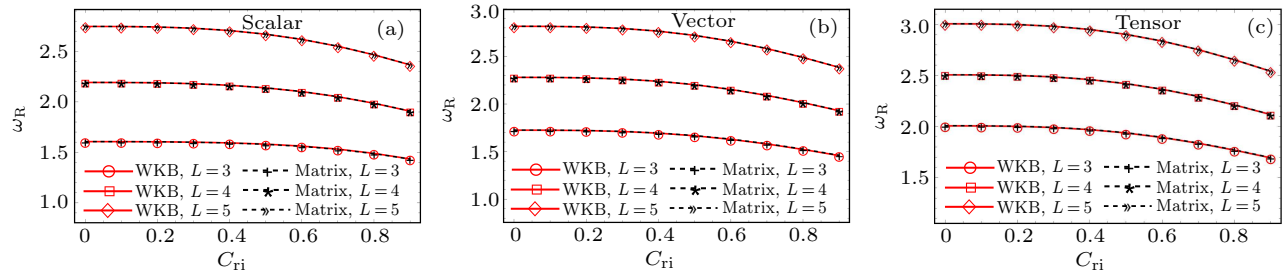


Fig. 13. The real part of the scalar-type (a), vector-type (b), and tensor-type (c) gravitational QNMs varies with the parameter C_{ri} for Case B with $r_p = 1$ and $n = 0$.

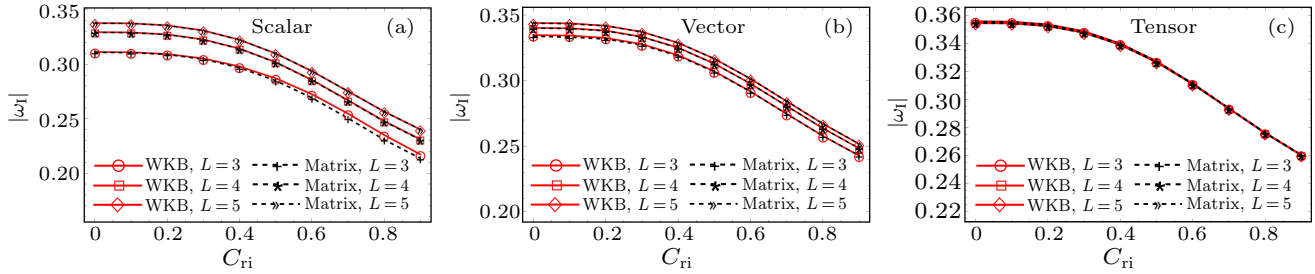


Fig. 14. The absolute value of the imaginary part of the scalar-type (a), vector-type (b), and tensor-type (c) gravitational QNMs varies with the parameter C_{ri} for Case B with $r_p = 1$ and $n = 0$.

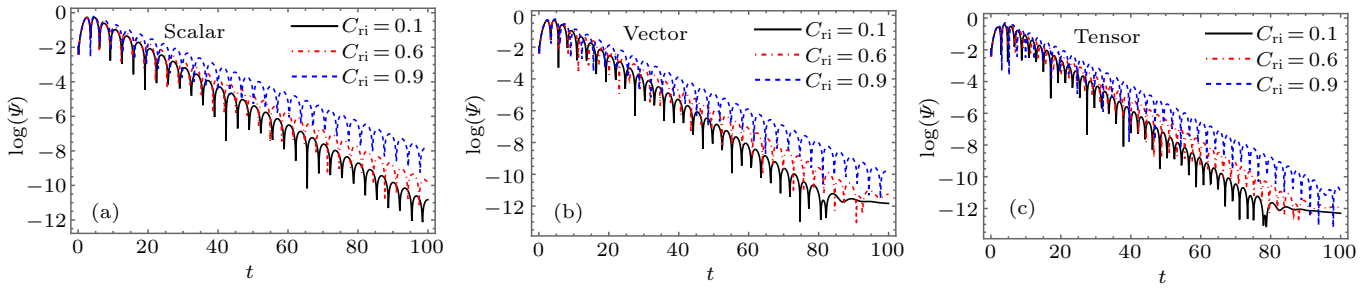


Fig. 15. Wave function images of the scalar-type (a), vector-type (b), and tensor-type (c) gravitational perturbation for Case B with $r_p = 1$ and $L = 2$.

Table 3. The scalar-type gravitational QNMs obtained by WKB approximation methods and matrix method for extreme black holes of case B with $r_p = 1$.

L	n	ω (third-order WKB)	ω (sixth-order WKB)	ω (matrix method)
2	0	0.82011 – 0.153007i		0.885497 – 0.174472i
3	0	1.36932 – 0.204358i	1.3991 – 0.182496i	1.368079 – 0.201033i
	1	1.32832 – 0.626066i	1.43246 – 0.488i	1.315202 – 0.612388i
	2	1.26639 – 1.07372i	1.06781 – 1.00237i	1.078321 – 1.023714i
4	0	1.82006 – 0.218233i	1.82143 – 0.217137i	1.820628 – 0.217876i
	1	1.77181 – 0.66187i	1.77859 – 0.650632i	1.771613 – 0.660262i
	2	1.68389 – 1.12332i	1.69839 – 1.07108i	1.711764 – 1.055638i
5	0	2.25672 – 0.22704i	2.25732 – 0.226994i	2.257210 – 0.227067i
	1	2.21255 – 0.685351i	2.2147 – 0.684371i	2.220545 – 0.683964i
	2	2.1281 – 1.15512i	2.12927 – 1.15198i	2.026350 – 1.046163i

Table 4. The vector-type gravitational QNMs obtained by WKB approximation methods and matrix method for extreme black holes of case B with $r_{\rm p} = 1$.

L	n	ω (third-order WKB)	ω (sixth-order WKB)	ω (matrix method)
2	0	0.907365 – 0.228664i	0.898659 – 0.222089i	0.912287 – 0.223176i
	1	0.774508 – 0.718504i	0.707265 – 0.727503i	0.788703 – 0.683480i
3	0	1.38874 – 0.230199i	1.3927 – 0.229234i	1.391606 – 0.230247i
	1	1.30371 – 0.702421i	1.32097 – 0.690864i	1.313412 – 0.698207i
	2	1.14771 – 1.20404i	1.17321 – 1.16276i	1.293748 – 1.101238i
4	0	1.8389 – 0.235482i	1.84024 – 0.235467i	1.840099 – 0.235504i
	1	1.77756 – 0.713189i	1.7831 – 0.711803i	1.786581 – 0.717272i
	2	1.66182 – 1.20856i	1.66879 – 1.20547i	1.631257 – 1.053548i
5	0	2.27276 – 0.238643i	2.27346 – 0.23865i	2.273340 – 0.238827i
	1	2.22371 – 0.720379i	2.22648 – 0.719867i	2.234107 – 0.709720i
	2	2.1296 – 1.21422i	2.13248 – 1.21345i	1.909996 – 1.067888i

Table 5. The tensor-type gravitational QNMs obtained by WKB approximation methods and matrix method for extreme black holes of case B with $r_{\rm p} = 1$.

L	n	ω (third-order WKB)	ω (sixth-order WKB)	ω (matrix method)
2	0	1.20874 – 0.247474i	1.21354 – 0.24798i	1.213607 – 0.247831i
	1	1.10753 – 0.765545i	1.12283 – 0.761169i	1.124900 – 0.755233i
3	0	1.61401 – 0.246924i	1.61612 – 0.247049i	1.616142 – 0.247008i
	1	1.54033 – 0.752116i	1.54776 – 0.750364i	1.541467 – 0.752439i
	2	1.40754 – 1.28391i	1.41231 – 1.2838i	1.491306 – 1.144148i
4	0	2.01792 – 0.246645i	2.01902 – 0.246689i	2.018902 – 0.246636i
	1	1.96019 – 0.746643i	1.96421 – 0.745845i	1.973650 – 0.752631i
	2	1.85196 – 1.26391i	1.85496 – 1.26344i	1.780672 – 1.076500i
5	0	2.42146 – 0.246484i	2.42209 – 0.246504i	2.421931 – 0.246749i
	1	2.37398 – 0.743891i	2.37637 – 0.743487i	2.385457 – 0.727910i
	2	2.28311 – 1.25329i	2.28505 – 1.25295i	2.020183 – 1.083491i

Case B We also performed numerical simulations using the finite difference method for different inner horizon positions: $r_{\rm i}$ taken at $0.1 \cdot r_{\rm p}$, $0.6 \cdot r_{\rm p}$, and $0.9 \cdot r_{\rm p}$. The resulting waveforms are shown in Fig. 15. As expected, with an increasing inner horizon, the oscillation frequency decreases, and the amplitudes decay more slowly. This is consistent with the results calculated using the WKB approximation method and the matrix method.

Case B Additionally, we applied the WKB approximation methods and matrix methods to extreme black holes. The results, summarized in Tables 3, 4, and 5, correspond to scalar-type, vector-type, and tensor-type gravitational QNMs. We found that the real part of the QNMs decreases as the overtone n increases, and the absolute value of the imaginary part increases as n increases. This behavior indicates that the oscillation frequency decreases with increasing n, and the amplitudes decay more rapidly as n increases.

5. Conclusion

In this article, we investigated the gravitational QNMs of charged Rastall black holes surrounded by quintessence fluid in both 4D and 5D spacetimes. In the 4D case, we first consider the impact of charge Q on the QNMs. We find that as the charge Q of the black hole increases, the gravitational oscillation frequency decreases, and the amplitudes decay more slowly. Next, we consider the effect of the parameter $C_{\rm a}$ on the QNMs. We divide the solutions into two different cases based on the properties of the horizons which are governed by $f(r) = 0$. When the black hole with only one event horizon, we find that the oscillation frequency decreases as the parameter $C_{\rm a}$ increases, and the amplitude decay more slowly as the parameter $C_{\rm a}$ increases. When the black hole has two horizons, we find that the oscillation frequency decreases as the inner horizon increases, and the amplitude decay more slowly as the inner horizon increases. We also explored extreme black holes and found that the oscillation frequency decreases with the overtone n increases, while the amplitudes decay more rapidly with increasing n. In the 5D spacetime, we consider the impact of the parameter $C_{\rm a}$ on the QNMs. We find that the behavior of gravitational QNMs for Rastall black holes surrounded by quintessence fluid in 5D spacetime is similar to that in 4D spacetime.

Acknowledgements

Project supported by the National Natural Science Foundation of China (Grant No. 42230207) and the Fundamental

Research Funds for the Central Universities, China University of Geosciences (Wuhan) (Grant No. G1323523064).

References

[1] Weber J 1960 *Phys. Rev.* **117** 306
[2] Abbott B P, Abbott R, Abbott T D, *et al*. 2016 *Phys. Rev. Lett.* **116** 061102
[3] Garcia-Quiros C, Colleoni M and Husa S, *et al*. 2020 *Phys. Rev. D* **102** 064002
[4] Ellis J, Lewicki M, No J M and Vaskonen V 2019 *J. Cosmol. Astropart. Phys.* **2019** 024
[5] Yan R and Lau Y K 2023 *Chin. Phys. Lett.* **40** 100401
[6] Abbott B P, Abbott R and Abbott T D, *et al*. 2017 *Class. Quantum Grav.* **34** 044001
[7] Taiji Sci Collaboration collaboration, Wu Y L, Luo Z R and Wang J Y, *et al*. 2021 *Commun. Phys.* **4** 34
[8] Mei J, Bai Y Z, Bao J, *et al.* 2020 *Prog. Theor. Exp. Phys.* **2021** 05A107
[9] Einstein A 1915 *Sitzungsberichte der Königlich Preussischen Akademie der Wissenschaften* 831
[10] Schwarzschild K 1916 *Sitzungsberichte der Königlich Preussischen Akademie der Wissenschaften* 189
[11] Perlmutter S, Aldering G, Goldhaber G, *et al*. 1999 *Astrophys. J.* **517** 565
[12] Riess A G, Filippenko A V, Challis P, *et al*. 1998 *Astron. J.* **116** 1009
[13] Riess A G, Strolger L G, Tonry J, *et al*. 2004 *Astrophys. J.* **607** 665
[14] Dodelson S and Widrow L M 1994 *Phys. Rev. Lett.* **72** 17
[15] Cole S, Aragon-Salamanca A, Frenk C S, Navarro J F and Zepf S E 1994 *Mon. Not. R. Astron. Soc.* **271** 781
[16] Rastall P 1972 *Phys. Rev. D* **6** 3357
[17] Lin K, Liu Y and Qian W L 2019 *Gen. Rel. Grav.* **51** 62
[18] De Felice A and Tsujikawa S 2010 *Living Rev. Rel.* **13** 3
[19] Sotiriou T P and Faraoni V 2010 *Rev. Mod. Phys.* **82** 451
[20] Kanti P, Mavromatos N E, Rizos J, Tamvakis K and Winstanley E 1996 *Phys. Rev. D* **54** 5049
[21] Antoniou G, Bakopoulos A and Kanti P 2018 *Phys. Rev. D* **97** 084037
[22] Kleihaus B, Kunz J, Mojica S and Radu E 2016 *Phys. Rev. D* **93** 044047
[23] Cunha P V P, Herdeiro C A R, Kleihaus B and Kunz J 2017 *Phys. Lett. B* **768** 373
[24] Blazquez-Salcedo J L, Khoo F S and Kunz J 2017 *Phys. Rev. D* **96** 064008
[25] Myrzakulov R 2011 *Eur. Phys. J. C* **71** 1752
[26] Zheng R and Huang Q 2011 *J. Cosmol. Astropart. Phys.* **2011** 002
[27] Jacobson T and Mattingly D 2001 *Phys. Rev. D* **64** 024028
[28] Horava P 2009 *Phys. Rev. D* **79** 084008
[29] Wang A 2017 *Int. J. Mod. Phys. D* **26** 1730014
[30] Lin K, Wang A, Wu Q and Zhu T 2011 *Phys. Rev. D* **84** 044051
[31] Bailin D and Love A 1987 *Rep. Progr. Phys.* **50** 1087
[32] Overduin J M and Wesson P S 1997 *Phys. Rep.* **283** 303
[33] Maartens R 2004 *Living Rev. Rel.* **7** 7
[34] Dick R 2001 *Class. Quantum Grav.* **18** R1
[35] Bergmann P G 1968 *Internat. J. Theoret. Phys.* **1** 25
[36] Wagoner R V 1970 *Phys. Rev. D* **1** 3209
[37] Oliveira A M, Velten H E S, Fabris J C and Casarini L 2015 *Phys. Rev. D* **92** 044020
[38] Moradpour H, Sadeghnezhad N and Hendi S H 2017 *Can. J. Phys.* **95** 1257
[39] Moradpour H and Salako I G 2016 *Adv. High Energy Phys.* **2016** 3492796
[40] Heydarzade Y and Darabi F 2017 *Phys. Lett. B* **771** 365
[41] Heydarzade Y, Moradpour H and Darabi F 2017 *Can. J. Phys.* **95** 1253
[42] Hansraj S and Banerjee A 2018 *Phys. Rev. D* **97** 104020
[43] Hansraj S, Banerjee A and Channuie P 2019 *Ann. Phys.* **400** 320
[44] Moradpour H, Sadeghnezhad N, Ghaffari S and Jahan A 2017 *Adv. High Energy Phys.* **2017** 9687976
[45] Zhu X R, Chen Y X, Mou P H and He K J 2023 *Chin. Phys. B* **32** 010401
[46] Ditta A, Xia T, Mahmood I and Mahmood A 2024 *Chin. Phys. B* **33** 030204
[47] Ziaie A H, Moradpour H and Ghaffari S 2019 *Phys. Lett. B* **793** 276
[48] De Moraes W A G and Santos A F 2019 *Gen. Rel. Grav.* **51** 167
[49] Shabani H and Hadi Ziaie A 2020 *Europhys. Lett.* **129** 20004
[50] Al-Rawaf A S and Taha M O 1996 *Phys. Lett. B* **366** 69
[51] Batista C E M, Daouda M H, Fabris J C, Piattella O F and Rodrigues D C 2012 *Phys. Rev. D* **85** 084008
[52] Fabris J C, Piattella O F and Rodrigues D C Batista C E M and Daouda M H 2012 *Int. J. Mod. Phys. Conf. Ser.* **18** 67
[53] Bronnikov K A, Fabris J C, Piattella O F and Santos E C 2016 *Gen. Rel. Grav.* **48** 162
[54] Batista C E M, Fabris J C, Piattella O F and Velasquez-Toribio A M 2013 *Eur. Phys. J. C* **73** 2425
[55] Moradpour H, Heydarzade Y, Darabi F and Salako I G 2017 *Eur. Phys. J. C* **77** 259
[56] Vishveshwara C V 1970 *Nature* **227** 936
[57] Gundlach C, R. Price H and Pullin J 1994 *Phys. Rev. D* **49** 883
[58] Leaver E W 1985 *Proc. R. Soc. Lond. A* **402** 285
[59] Iyer S and Will C M 1987 *Phys. Rev. D* **35** 3621
[60] Konoplya R A 2003 *Phys. Rev. D* **68** 024018
[61] Matyjasek J and Opala M 2017 *Phys. Rev. D* **96** 024011
[62] Konoplya R A, Zhidenko A and Zinhailo A F 2019 *Class. Quantum Grav.* **36** 155002
[63] Matyjasek J and Telecka M 2019 *Phys. Rev. D* **100** 124006
[64] Lin K and Qian W L 2017 *Class. Quantum Grav.* **34** 095004
[65] Lin K, Qian W L, Pavan A B and Abdalla E 2017 *Mod. Phys. Lett. A* **32** 1750134
[66] Lin K and Qian W L 2019 *Chin. Phys. C* **43** 035105
[67] Kim S W, Nishimura J and Tsuchiya A 2012 *Phys. Rev. Lett.* **108** 011601
[68] Pius R and Sen A 2016 *J. High Energy Phys.* **2016** 24
[69] Sen A 2018 *J. High Energy Phys.* **2018** 155
[70] Giddings S B and Thomas S 2002 *Phys. Rev. D* **65** 056010
[71] Born M and Infeld L 1934 *Proc. Roy. Soc. Lond. A* **143** 410
[72] Hoffmann B 1935 *Phys. Rev.* **47** 877
[73] Hendi S H 2009 *Phys. Lett. B* **677** 123
[74] Hendi S H 2011 *Eur. Phys. J. C* **71** 1551
[75] Zlatev I, Wang L M and Steinhardt P J 1999 *Phys. Rev. Lett.* **82** 896
[76] Amendola L 2000 *Phys. Rev. D* **62** 043511
[77] Scherrer R J 2004 *Phys. Rev. Lett.* **93** 011301
[78] Padmanabhan T and Roy Choudhury T 2002 *Phys. Rev. D* **66** 081301
[79] Nojiri S and Odintsov S D 2003 *Phys. Lett. B* **565** 1
[80] Feng B, Wang X and Zhang X 2005 *Phys. Lett. B* **607** 35
[81] Graca J P M and Lobo I P 2018 *Eur. Phys. J. C* **78** 101
[82] Regge T and Wheeler J A 1957 *Phys. Rev.* **108** 1063
[83] Zerilli F J 1970 *Phys. Rev. Lett.* **24** 737
[84] Moncrief V 1974 *Ann. Phys.* **88** 323
[85] Teukolsky S A 1973 *Astrophys. J.* **185** 635
[86] Takahashi T and Soda J 2010 *Prog. Theor. Phys.* **124** 911